THE JOURNAL OF PHYSICAL CHEMISTRY C

Article

Cite This: J. Phys. Chem. C 2018, 122, 15190−15197

pubs.acs.org/JPCC

Study on the Photoresponse Characteristics of Organic Light-Emitting Field-Effect Transistors

Dongwei Li,[†,‡] Yongsheng Hu,[*,†] Xiaoyang Guo,[†] Ying Lv,[†] Nan Zhang,[†] Jie Lin,[†] and Xingyuan Liu[*,†]

[†]State Key Laboratory of Luminescence and Applications, Changchun Institute of Optics, Fine Mechanics, and Physics, Chinese Academy of Sciences, Changchun 130033, China

[‡]University of Chinese Academy of Sciences, Beijing 100049, China

Supporting Information

ABSTRACT: Organic photodetectors have attracted great attention because of their promising applications in the fields of imaging, optical communication, and biosensing. Although the optical and electrical performances of the organic light-emitting field effect transistors (OLEFETs) have improved substantially in the past decade, the photodetection property of the OLEFETs has rarely been studied. Here, we investigated the photoresponse characteristics of the hetero-structured OLEFETs, which unexpectedly shows performance comparable to some organic phototransistor-only devices, without sacrificing the light emission performance of the device. The device shows photoresponse ability in a wide visible light range and a maximum photon-to-electron efficiency of 45 300% with millisecond-scale switching on and off time when under the illumination of 405 nm. It is found that the photoresponse characteristics of the devices are mainly determined by the hole injection layer, as light absorption happens mainly in this layer. Our study would provide some insights into further exploring the light detection potential for the multifunctional OLEFETs, which might meet the requirements for future high integration, low-weight, and low-cost applications.

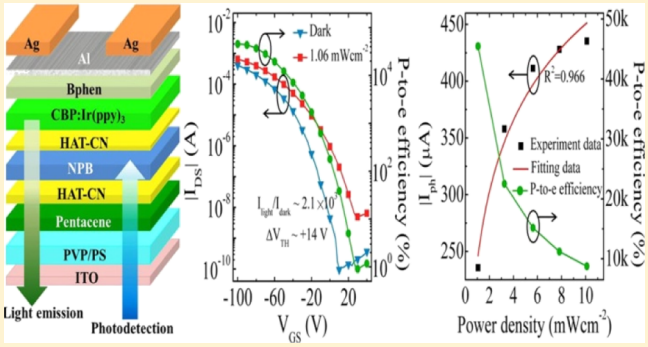

1. INTRODUCTION

Organic photodetectors have attracted great attention because of their promising applications in the fields of imaging, optical communication, and biosensing.[1−3] Thereinto, organic phototransistors (OPTs) have shown great advantage in achieving high photon-to-electron (p-to-e) efficiency because of the basic structure of organic field effect transistors (OFETs), which enables signal amplification (gain) without increasing the noise.[4,5] For instance, remarkable performances have been achieved for OPTs by employing a wide variety of active materials including not only small molecules[6,7] and polymers[8,9] but also hybrids with materials such as quantum dots,[10−12] two-dimensional materials,[13,14] and the newly emerged perovskite.[15,16]

Organic light-emitting field effect transistors (OLEFETs) are a novel kind of multifunctional optoelectronic devices that integrate both the switching function of OFETs and the luminescence function of organic light-emitting diodes (OLEDs),[17] which have shown promising applications in the fields of flat panel displays, integrated optical interconnection, and optical communication.[18−20] In the past decade, the optical [external quantum efficiency (EQE) and brightness] and electrical (mobility and on−off ratio) performances of OLEFETs have improved substantially as a result of the development of various kinds of novel materials[21,22] and device architectures,[23−25] especially the multilayered heterostructure[23,26] that enables much flexibility in incorporating an emission layer with high emission efficiency and a charge-transport layer with high carrier mobility simultaneously. However, it is worth noting that few studies have been reported on the photoresponse characteristics of the OLEFETs up to now.

In principle, it is challenging to realize light detection and light emission concurrently in a single OLEFET because of the fact that the energy conversion between photons and electrons is inverse for the two processes, which will inevitably result in quite different requirements for the organic active materials as well as for the device architectures. For instance, organic active materials with high carrier mobility and good light absorption are necessary for the OPTs,[14,27] whereas balanced carrier transport and high photoluminescence quantum efficiency are more crucial for the OLEFETs.[25,28] Nevertheless, considering the basic structure of OFETs, OLEFETs may still become a good kind of OPT with high gain. Recently, we have reported an OLEFET-based near-infrared (NIR)-to-visible upconver-

Received: May 6, 2018
Published: June 13, 2018

DOI: 10.1021/acs.jpcc.8b04320
J. Phys. Chem. C 2018, 122, 15190−15197

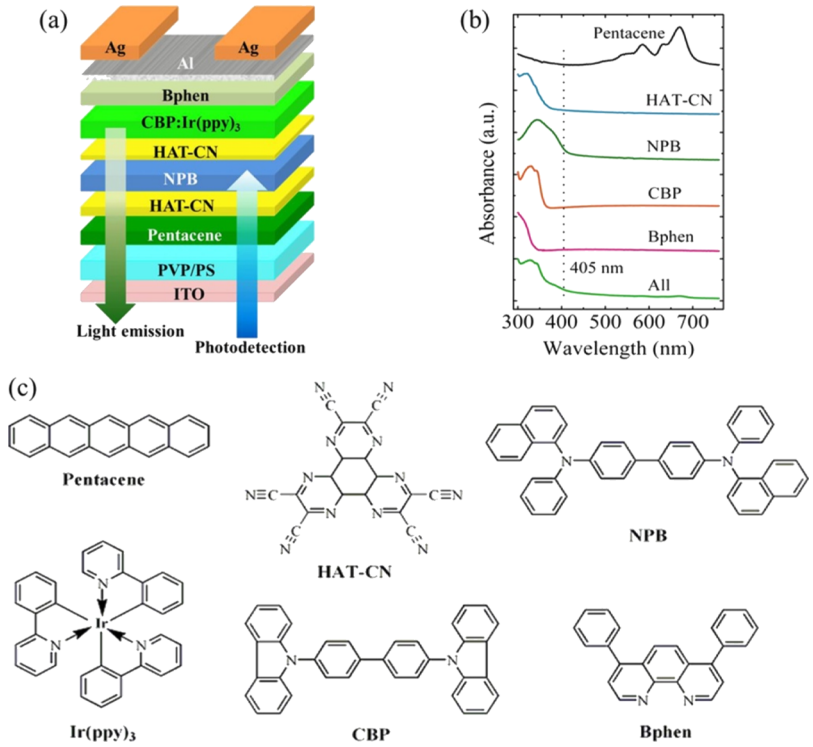

Figure 1. (a) Schematic of the OLEFETs. The green and blue arrows indicate the output direction for light emission and the input direction of the incident light for photodetection, respectively. (b) Absorption spectra of each active layer and the whole active layers (denoted as "All"). The dashed line is the guidance for the position of 405 nm. (c) Molecular structures of the active materials.

sion device without sacrificing the light emission performance of the device, demonstrating a promising light detection potential for the OLEFETs.[29]

In this work, we focus on the photoresponse characteristics of heterostructured OLEFETs. The devices exhibit notable photodetection ability in a wide visible light range. Surprisingly, a maximum p-to-e efficiency as high as 45 300%, which is comparable with some OPT-only devices, can be obtained when under illumination of 405 nm with 1.06 mW cm^{-2}. Besides, the devices show good photoswitching behaviors with millisecond-scale response time. It is revealed that the photoresponse characteristics are mainly influenced by the hole injection layer. Our study would provide some insights into further exploring the light detection potential of the OLEFETs, which might meet the requirements for future high integration, low-weight, and low-cost applications.

2. EXPERIMENTAL SECTION

The schematic of the device is shown in Figure 1a. Indium tin oxide (ITO) on a glass substrate was used as the gate electrode. Poly-4-vinylpenol (350 nm) and 30 nm polystyrene, prepared by spin-coating in a method reported elsewhere,[30] were used as the dielectric (capacitance $C_i \approx 7.5$ nF cm^{-2}). Pentacene, *N*,*N*′-di(naphthalene-1-yl)-*N*,*N*′-diphenyl-benzidine (NPB), 4,4′-bis(carbazol-9-yl)biphenyl:Fac-tris(2-phenylpyridinato)iridium(III) (CBP:Ir$(ppy)_3$), and bathophenanthroline (Bphen) act as the hole transport layer, hole injection layer, emission layer, and electron injection layer, respectively. The n/p/n interfacial layer, which consists of 1,4,5,8,9,11-hexaazatriphenylene hexacarbonitrile (HAT-CN)/NPB/HAT-CN, plays the role of hole generation[21] that could facilitate the drain current (I_{DS}) and hole injection into the emission layer and thereby greatly promote the brightness and EQE of the OLEFETs. The molecular structures of the organic materials are presented in Figure 1c. Pentacene (12 nm), HAT-CN (2 nm), NPB (x nm), HAT-CN (1 nm), CBP:Ir$(ppy)_3$ (25 nm, weight concentration of approximately 6%), and Bphen (14 nm) were successively evaporated at the rates of 0.15, 0.05, 0.15, 0.05, 1.6, and 0.2 Å/s, respectively. Al (1 nm) was evaporated to further promote electron injection before the 100 nm Ag source/drain electrodes with the channel length and width of 45 and 3000 μm, respectively. The devices were encapsulated in the glovebox (H_2O, O_2 < 0.1 ppm) before the test. The light emission is collected from the ITO side when the device is operating in the light emission mode, whereas the incident light is illuminated from the ITO side when the device is operating in the photodetection mode.

The electrical characteristics were performed by a Keithley 4200 SCS system at room temperature under ambient air. The photocurrent (I_{ph}) was recorded by a Hamamatsu S1336 photodiode. A high pass optical filter of 455 nm was put in front of the photodiode to avoid scattering of the incident light when measuring the light emission intensity under illumination. The image of light emission was captured by an Olympus BX51TRF CCD microscope with a 20× objective lens. The incident light sources for the photodetection test were four different lasers (continuous wave) with wavelengths of 405, 457, 532, and 650 nm. The intensity of the light sources was adjusted by a set of calibrated neutral density filters, whereas the power was recorded using a Thorlabs PM320E optical power and energy meter. The absorption spectra were measured by a UV-3101PC ultraviolet (UV)−visible−NIR spectrophotometer. The carrier mobility was calculated by the formula for the saturation regime: $I_{DS} = \mu C_i(W/2L)(V_{GS} - V_{TH})^2$ (where μ is the field-effect mobility, C_i is the gate dielectric capacitance density, V_{TH} is the threshold voltage, and

DOI: 10.1021/acs.jpcc.8b04320
J. Phys. Chem. C 2018, 122, 15190−15197

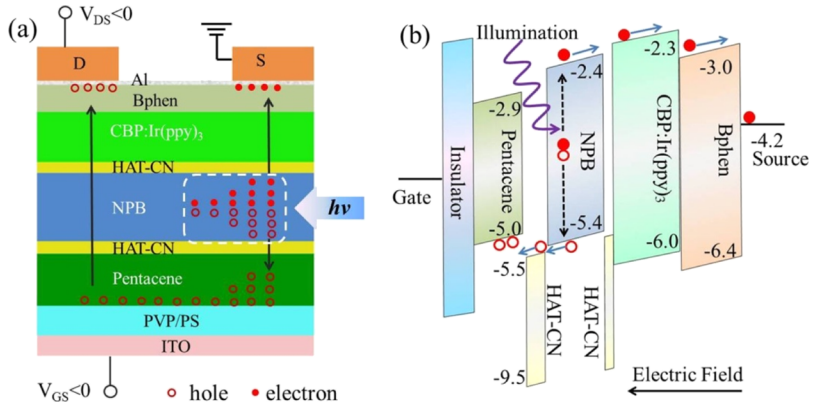

Figure 2. Photodetection mechanism of the device. (a) Schematic of the carrier transport. (b) Schematic of the energy level diagram for the photogenerated carriers transporting under the source electrode.

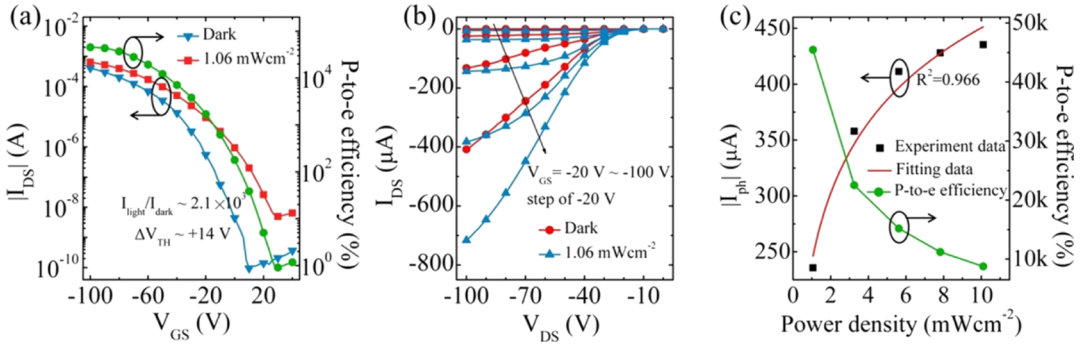

Figure 3. Photoresponse characteristics of the devices under the incident light of 405 nm. (a) Transfer curves and the corresponding p-to-e efficiency at V_{DS} = −80 V, with and without illumination. (b) Output curves with and without illumination. (c) Measured and fitted results of the photocurrent at different incident light intensities and the corresponding p-to-e efficiency at V_{GS} = −100 V and V_{DS} = −80 V.

W and L are the channel width and length, respectively). The brightness was calculated by comparing the photocurrent with a standard OLED of known brightness (1000 cdm^{-2}) and emission area (3 mm × 1 mm) with the structure of ITO/NPB/CBP:Ir(ppy)$_3$/Bphen/LiF/Al. The EQE was calculated from the brightness, the drain current, and the electroluminescent emission spectrum, assuming Lambertian emission. The detectivity was calculated by the formula,[31,32] $D^* = R\sqrt{A}/S_N = R\sqrt{A}/\sqrt{2qI_{dark}}$ (S_N is the current spectral noise density, S_N^2 is the sum of all noise power, and A is the device area).

3. RESULTS AND DISCUSSION

Figure 1b shows the absorption spectra of each active layer as well as the whole active layers (denoted as "All"). The absorption of the whole active layers is mainly located below 450 nm, which is consistent with that for each active layer. There is a weak absorption band around 670 nm for the whole active layers, which should be originated from pentacene, as only the film of pentacene shows distinguishable absorption in this range. At the wavelength of 405 nm (wavelength of one of the incident light sources), absorption can be observed only for the film of NPB. Although additional absorption bands around 405 nm can also be aroused from the charge-transfer process between HAT-CN and pentacene,[21] considering the ultrathin thickness of HAT-CN, we can roughly neglect the absorption caused by HAT-CN. Therefore, when illuminated under the light of 405 nm, the light absorption and thereby the generation of excitons should happen mainly in the hole injection layer of NPB. Actually, NPB shows a relatively high absorption coefficient of ~5 × 10^4 cm^{-1} at 405 nm (calculated from the absorbance, shown in Figure S1) and is believed to be a promising photosensitive material,[33,34] in addition to the wide usage in the OLEDs.

Figure 2 illustrates the photodetection working mechanism of the device. Because of the hole dominated property of pentacene, the device is generally biased under a gate to source voltage (V_{GS}) < 0 V and a drain to source voltage (V_{DS}) < 0 V to ensure the hole accumulation mode. As shown in Figure 2a, the incident light is mainly absorbed in NPB followed by the generation of the photogenerated excitons. The photogenerated excitons can be separated into electrons and holes more efficiently near the source electrode because of the vertical electric field. The electrons will move across CBP:Ir(ppy)$_3$ and Bphen layers and accumulate under the source electrode, where they can effectively lower the hole injection barrier at the source electrode, resulting in an effective decrease in the contact resistance and in a positive shift of V_T;[35,36] whereas the holes will move down to pentacene and accumulate in the channel, followed by transporting along the interface of dielectric/pentacene toward the drain electrode because of the horizontal electric field effect, and finally be collected by the drain electrode to form the photogenerated current. Figure 2b shows the corresponding energy level diagram under the source electrode. It is worth mentioning that the separation of the photogenerated excitons will not impact the radiative recombination of excitons in the emission layer because the latter mainly occurs under the drain

DOI: 10.1021/acs.jpcc.8b04320
J. Phys. Chem. C 2018, 122, 15190−15197

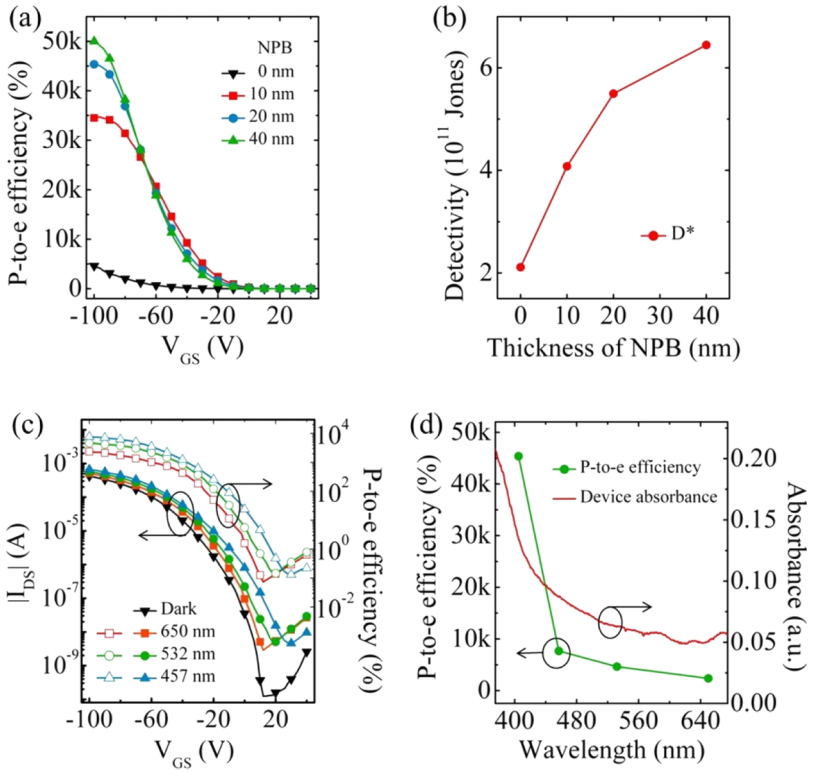

Figure 4. (a) p-to-e efficiency of the devices with different thicknesses of NPB at V_{DS} = −80 V. (b) Detectivity of the devices with different thicknesses of NPB. (c) Photoresponse characteristics of the device with 20 nm NPB at V_{DS} = −80 V when illuminated under the incident light of 650, 532, and 457 nm (power density is 1 mW cm^{-2}). (d) Comparison of the p-to-e efficiency and absorption spectra of the device with 20 nm NPB.

electrode.[30] In this way, light emission and photodetection can be achieved concurrently in a single OLEFET.

Figure 3a shows the transfer curves of the device both in the dark and under illumination as well as the corresponding p-to-e efficiency at V_{DS} = −80 V. The wavelength and power density of the illuminated light was 405 nm and 1.06 mW cm^{-1}, respectively. In the dark, the device exhibits a typical p-type characteristic with a hole mobility of 0.65 cm^2 V^{-1} s^{-1}, on−off ratio > 10^6, and V_T = −33 V. When the device is under illumination, the drain current changes significantly, indicating that a large number of photogenerated excitons have been produced and separated effectively, concurrent with a positively shifted V_{TH} of 14 V. The maximum ratio of the drain current between under illumination and in the dark (I_{light}/I_{dark}) reaches about 2.1 × 10^3 around V_{GS} = 10 V when the device is in the off-state where the photocurrent is dominated. To elucidate the photoresponse performance of the devices, we calculated the p-to-e efficiency represented as η by the following formula[37]

$$\eta = \frac{hc}{q\lambda}R = \frac{hcI_{ph}}{q\lambda P_{inc}} = \frac{hc(I_{light} - I_{dark})}{q\lambda P_{inc}} \quad (1)$$

where $\frac{hc}{\lambda}$ is the photon energy, q is the electron charge, R is the photoresponsivity, I_{light} is the drain current under illumination, I_{dark} is the drain current in the dark, and P_{inc} is the incident light power on the channel area. As shown in Figure 3a, with V_{GS} increasing negatively from 20 to −100 V, the p-to-e efficiency increases first and tends to saturation after V_{GS} reaches −90 V. The saturation indicates that most photogenerated excitons have been separated and collected under the high electric field. The maximum p-to-e efficiency of the device reaches over 45 300%, which is comparable with some OPT-only devices in the literature.[38,39] The high p-to-e efficiency can be attributed to the good combination of the high absorbance of the photosensitive layer (NPB) and the high mobility of the transporting layer (pentacene), which are actually the key factors for efficient heterostructured OPT-only devices.[40] The much higher than 100% of the p-to-e efficiency also signifies the gain mechanism for the OFET-based device structure.[41] Figure 3b gives the output characteristic of the devices, which again shows a distinct increase of I_{DS} under illumination than in the dark for the V_{GS} range from −20 to −100 V. Similarly, as V_{DS} increases negatively, the photocurrent improves remarkably, which is reasonable because the increased horizontal electric field would accelerate the transportation of the photogenerated holes in the channel, as described in Figure 2a.

The photocurrent and p-to-e efficiency as functions of the incident light power density are shown in Figure 3c. For OPT-only devices, the drain current under the on-state ($|V_{GS}| > |V_{TH}|$) is mainly governed by the photovoltaic effect, and the relationship between $I_{ph.on}$ and P_{inc} can expressed by the formula[5,40]

$$I_{ph.on} = g_m \Delta V_T = \frac{AkT}{q} \ln\left(1 + \frac{\eta q \lambda P_{inc}}{I_{dark} hc}\right) \quad (2)$$

where $g_m = dI_{DS}/dV_{GS}$ represents the transconductance of the devices, A is a proportionality parameter, k is the Boltzmann constant, T is the operating temperature, λ is the wavelength of the incident light, η is the p-to-e efficiency, h denotes Planck's constant, and P_{inc} is the incident light power. The experimental

DOI: 10.1021/acs.jpcc.8b04320
J. Phys. Chem. C 2018, 122, 15190−15197

Table 1. Summary of the Photoresponse and Light Emission Characteristics of the Devices

		photoresponse characteristic			light emission characteristic	
devices NPB (nm)	incident light (nm)	max p-to-e efficiency (%)	max photoresponsivity (A W^{-1})	max photosensitivity	max brightness (cdm^{-2})	EQE at max brightness (%)
0	405	4620	15 ± 0.8	120 ± 10	299 ± 50	1.40 ± 0.1
10	405	34 510	113 ± 5	1400 ± 100	8337 ± 300	4.77 ± 0.3
20	405	45 300	148 ± 5	2100 ± 200	6324 ± 300	5.65 ± 0.3
40	405	49 990	163 ± 10	2360 ± 200	2730 ± 200	6.40 ± 0.3
20	457	7670	28.2 ± 1	740 ± 80		
20	532	4640	19.8 ± 1	130 ± 10		
20	650	2365	12.3 ± 0.8	40 ± 5		

data of the device can be well-fitted with the above relationship, which implies that the photodetection of OLEFETs also follows photovoltaic effect when under the on-state.

The photoresponse characteristics of OPTs can also be characterized by the photoresponsivity (R) and photosensitivity (P) with $R = (I_{light} - I_{dark})/P_{inc}$ and $P = (I_{light} - I_{dark})/I_{dark}$. The R and P curves versus V_{GS} derived from Figure 3a are shown in Figure S2. The maximum R and P reaches 148 A W^{-1} and 2.1×10^3. Although the value of R is high enough, the value of P has a big room to improve, especially at the region where R reaches the maximum. This might be viable by decreasing the dark current through methods such as introducing a hole block layer.[42]

We further investigated the influence of the thickness of the NPB layer on the photoresponse characteristics of the devices. Figure 4a shows the p-to-e efficiency with different thicknesses (0, 10, 20, and 40 nm) of NPB. The p-to-e efficiency improves from 4620 to 49 990% with the increase in the thickness of NPB, which means a substantial promotion of the population of the photogenerated excitons. The devices without NPB also exhibit a certain extent of photoresponse characteristic, which implies that light absorption can happen not merely in the NPB layer. Nevertheless, the more than 1 order of magnitude promotion of the p-to-e efficiency firmly manifests the crucial role of NPB in the photoelectric conversion process. Figure 4b shows that the detectivity (D^*) of devices with different thicknesses of NPB is on the order of 10^{11} Jones and increases with the increase in the thickness of NPB. It should be mentioned that the thickness of NPB will also obviously influence the light emission characteristics of the devices as a result of the change of the carrier balance. As listed in Table 1, the EQE improves from 4.77 to 6.4%, with the thickness of the NPB layer increasing from 10 to 40 nm, whereas the corresponding brightness declines from 8330 to 2700 cdm^{-2}. The detailed light emission characteristics with different thicknesses of NPB are presented in Figure S3.

An interesting phenomenon is that the device also exhibits moderate photoresponse performance in the wavelength region of beyond 450 nm despite weak light absorption. Figure 4c shows the transfer curves and the corresponding p-to-e efficiency of the device with 20 nm NPB illuminated under 650, 532, and 457 nm (the power density is about 1 mW cm^{-2}). V_{TH} shifts positively for 2, 5, and 8 V. The maximum p-to-e efficiencies are 2360, 4640, and 7670% and the corresponding maximum R and P values are 12.3 A W^{-1} and 40, 19.8 A W^{-1} and 130, and 28.2 A W^{-1} and 740 for illuminations of 650, 532, and 457 nm, respectively (Figure S4 and Table 1). The wavelength dependence of the p-to-e efficiency is in agreement qualitatively with the absorption spectrum of the device, as shown in Figure 4d. We have not performed the measurement for the UV region because of the test limitation, however, it can be anticipated that much better performance can be obtained as described for most OPTs in the literature,[34,43] owing to the higher absorbance of the active layers in the region. It is noteworthy that the utilization of NPB is not mandatory in the current device structure. Song et al. have reported efficient OLEFETs based on several different charge generation layers.[22] Therefore, it is possible to further improve the photoresponse performance and extend the photoresponse wavelength range by adopting hole injection layers with higher absorbance and wider absorption range.

Figure 5 shows the photoswitching behaviors of the device with 20 nm NPB under the incident light of 405 nm. The drain current changes promptly with the light on and off under different bias conditions. When under different V_{DS} (Figure 5a), the switching on and off time (from 10 to 90% of the drain

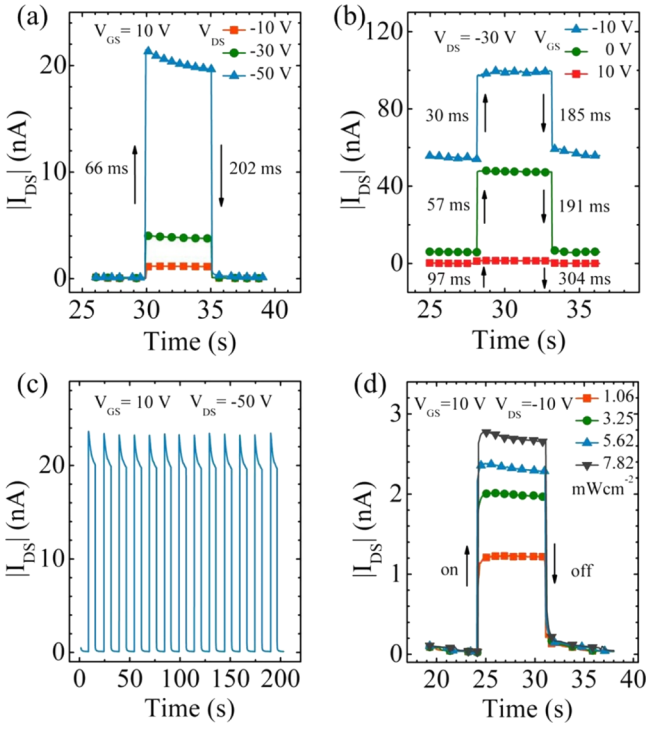

Figure 5. Photoswitching behaviors of the device. (a) Switching on and off property at V_{DS} = −10, −30, and −50 V with fixed V_{GS} = 10 V. (b) Switching on and off property at V_{GS} = −10, 0, and 10 V with fixed V_{DS} = −30 V. (c) Multicycle property at V_{GS} = 10 V and V_{DS} = −50 V. The power density of the illuminated light for (a−c) is fixed at 1.06 mW cm^{-2}. (d) Switching on and off property for different incident light intensities at V_{GS} = 10 V and V_{DS} = −10 V.

DOI: 10.1021/acs.jpcc.8b04320
J. Phys. Chem. C 2018, 122, 15190−15197

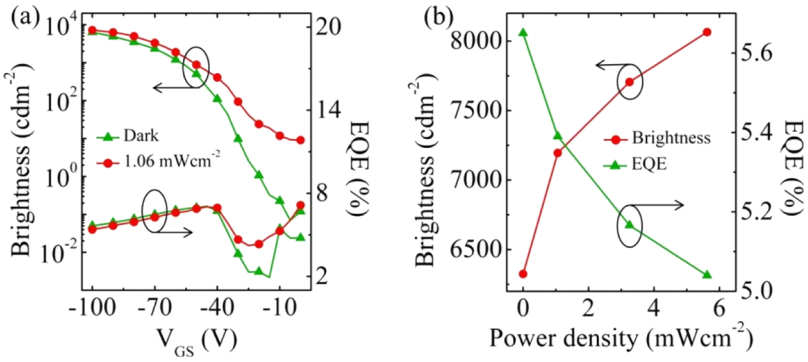

Figure 6. Influence of illumination on the light emission characteristics of the device. (a) Optical transfer curves both under illumination and in the dark at V_{DS} = −100 V. (b) Brightness and EQE at different power densities of the incident light with V_{DS} = −100 V and V_{GS} = −100 V.

current) at V_{GS} = 10 V is 66 and 202 ms, respectively, and shows no dependence on the biased V_{DS}. When V_{DS} is fixed, the switching on and off time is also in the range of tens to hundreds of milliseconds for different V_{GS} values (Figure 5b). However, it gets longer as V_{GS} increases positively, which can be attributed to the lower drift and diffusion rates of the photogenerated holes as the hole potential at the gate electrode raises.[44] Meanwhile, the persistent photocurrent (drain current when the illumination is off) is negligible for the device, indicating a relatively low concentration of trap states in the active layer.[4,45] Figure 5c presents the photoswitching behaviors over a long period of time for V_{GS} = 10 V and V_{DS} = −50 V. No degradation except for a small fluctuation at the moment when light is on can be observed. Figure 5d shows the switching on and off characteristic for different incident light intensities at V_{GS} = 10 V and V_{DS} = −10 V. Almost no variation of the rise and fall time is found, indicating rather good environmental operation stability for the device. The above photoswitching performance implies that the separation and collection of the photogenerated excitons have hardly been influenced by the multilayer structure, thus offering much flexibility for optimization of the device architecture in the future.

To further investigate the effect of light exposure on the light emission characteristics of the device, Figure 6 presents the optical transfer curves of the device both under illumination (405 nm) and in the dark. When under the illumination of 1.06 mW cm^{-2} (Figure 6a), the brightness increases, and a maximum brightness of 7190 cdm^{-2} can be reached compared to that of 6320 cdm^{-2} in the dark. The corresponding EQE at higher gate voltages (e.g., V_{GS} < −40 V) is slightly decreased. The increased brightness can be mainly attributed to the increase of the carrier density originated from the photogenerated excitons, as described previously. The decrease of EQE at high gate voltages probably results from the overbalance between holes and electrons at a high drain current. The higher EQE under illumination than that in the dark at lower gate voltages is likely to be caused by the photoluminescence, which can be dominated when there is little electroluminescence. However, the intensity of the photoluminescence is relatively weak, with a brightness of less than 10 cdm^{-2} estimated from the corresponding photocurrent of the photodiode. Figure 6b presents the brightness and EQE at different power densities of the incident light. As the incident light power density increases to 5.62 mW cm^{-2}, the brightness increases from 6320 to 8060 cdm^{-2}, whereas the corresponding EQE decreases slightly from 5.65 to 5.03%, which again indicates a compromise between the carrier density and balance transportation. Figure S5 presents the optical images of a working device with and without illumination under different bias conditions, from which a brighter emission can be seen for those with the illumination, however, with a relatively low contrast. Therefore, further studies are necessary to improve the photosensitivity of the device.

4. CONCLUSIONS

In conclusion, we have investigated the photoresponse characteristics of the multilayer heterostructured OLEFETs. It has been demonstrated that both good photodetection and light emission can be obtained in a single OLEFET. The device shows stronger emission when illuminated while the corresponding EQE suffers a slight decline as the illumination intensity increases. The hole injection layer of NPB plays an important role in determining the comprehensive performance of the devices, as the light absorption happens mainly in this layer. A maximum p-to-e efficiency of 45 300% and the switching on and off time within millisecond-scale range have been obtained when under the illumination of 405 nm. Further improvement of the performance as well as the reveal of the working mechanism are highly desired to boost the applications in fields such as multifunctional sensing and highly integrated optical interconnection for such devices.

■ ASSOCIATED CONTENT

Supporting Information

The Supporting Information is available free of charge on the ACS Publications website at DOI: 10.1021/acs.jpcc.8b04320.

Absorption coefficient of the active layers; photoresponsivity and photosensitivity of the devices under different illuminations; characteristics of brightness and EQE for the devices; and optical images of a working device with and without illumination (PDF)

■ AUTHOR INFORMATION

Corresponding Authors

*E-mail: huyongsheng@ciomp.ac.cn. Phone: +86-431-86176341 (Y.H.).

*E-mail: liuxy@ciomp.ac.cn. Phone: +86-431-86176342 (X.L.).

ORCID

Yongsheng Hu: 0000-0002-8116-4378

Xiaoyang Guo: 0000-0003-0259-137X

DOI: 10.1021/acs.jpcc.8b04320
J. Phys. Chem. C 2018, 122, 15190−15197

Ying Lv: 0000-0003-1649-5258
Jie Lin: 0000-0001-9676-2218
Xingyuan Liu: 0000-0002-9681-1646

Notes

The authors declare no competing financial interest.

■ ACKNOWLEDGMENTS

This work was funded by the CAS Innovation Program, the National Natural Science Foundation of China nos. 61775211, 61704170, and 51503196 and Jilin Province Science and Technology Research project nos. 20160520092JH, 20160520176JH, 20180201029GX, and 20170101039JC. The project was supported by the State Key Laboratory of Luminescence and Applications.

■ REFERENCES

(1) Zhang, L.; Wu, T.; Guo, Y.; Zhao, Y.; Sun, X.; Wen, Y.; Yu, G.; Liu, Y. Large-Area, Flexible Imaging Arrays Constructed by Light-Charge Organic Memories. *Sci. Rep.* **2013**, *3*, 1080.
(2) Park, J. H.; Lee, H. S.; Park, S.; Min, S.-W.; Yi, Y.; Cho, C.-G.; Han, J.; Kim, T. W.; Im, S. Photo-Stable Organic Thin-Film Transistor Utilizing a New Indolocarbazole Derivative for Image Pixel and Logic Applications. *Adv. Funct. Mater.* **2014**, *24*, 1109−1116.
(3) Lin, P.; Yan, F. Organic Thin-Film Transistors for Chemical and Biological Sensing. *Adv. Mater.* **2012**, *24*, 34−51.
(4) Baeg, K.-J.; Binda, M.; Natali, D.; Caironi, M.; Noh, Y.-Y. Organic Light Detectors: Photodiodes and Phototransistors. *Adv. Mater.* **2013**, *25*, 4267−4295.
(5) Dierckx, W.; Oosterbaan, W. D.; Bolsée, J.-C.; Cardinaletti, I.; Maes, W.; Boyen, H.-G.; D'Haen, J.; Nesladek, M.; Manca, J. Organic Phototransistors Using Poly(3-Hexylthiophene) Nanofibres. *Nanotechnology* **2015**, *26*, 065201.
(6) Qi, Z.; Cao, J.; Li, H.; Ding, L.; Wang, J. High-Performance Thermally Stable Organic Phototransistors Based on PSeTPTI/$PC_{61}BM$ for Visible and Ultraviolet Photodetection. *Adv. Funct. Mater.* **2015**, *25*, 3138−3146.
(7) Mukherjee, B. Large Photoresponse from a Small Molecule: Application in Photodetector and Pseudo-Transistor. *Optik* **2015**, *126*, 1258−1262.
(8) Nam, H. J.; Cha, J.; Lee, S. H.; Yoo, W. J.; Jung, D.-Y. A New Mussel-Inspired Polydopamine Phototransistor with High Photosensitivity: Signal Amplification and Light-Controlled Switching Properties. *Chem. Commun.* **2014**, *50*, 1458−1461.
(9) Gu, P.; Yao, Y.; Feng, L.; Niu, S.; Dong, H. Recent Advances in Polymer Phototransistors. *Polym. Chem.* **2015**, *6*, 7933−7944.
(10) Yu, H.; Kim, D.; Lee, J.; Baek, S.; Lee, J.; Singh, R.; So, F. High-Gain Infrared-to-Visible Upconversion Light-Emitting Phototransistors. *Nat. Photonics* **2016**, *10*, 129−134.
(11) Sun, Z.; Liu, Z.; Li, J.; Tai, G.-A.; Lau, S.-P.; Yan, F. Infrared Photodetectors Based on CVD-Grown Graphene and PbS Quantum Dots with Ultrahigh Responsivity. *Adv. Mater.* **2012**, *24*, 5878−5883.
(12) Gao, L.; Chen, C.; Zeng, K.; Ge, C.; Yang, D.; Song, H.; Tang, J. Broadband, Sensitive and Spectrally Distinctive SnS_2 Nanosheet/PbS Colloidal Quantum Dot Hybrid Photodetector. *Light: Sci. Appl.* **2016**, *5*, e16126.
(13) Huisman, E. H.; Shulga, A. G.; Zomer, P. J.; Tombros, N.; Bartesaghi, D.; Bisri, S. Z.; Loi, M. A.; Koster, L. J. A.; van Wees, B. J. High Gain Hybrid Graphene−Organic Semiconductor Phototransistors. *ACS Appl. Mater. Interfaces* **2015**, *7*, 11083−11088.
(14) Lee, Y.; Kwon, J.; Hwang, E.; Ra, C.-H.; Yoo, W. J.; Ahn, J.-H.; Park, J. H.; Cho, J. H. High-Performance Perovskite-Graphene Hybrid Photodetector. *Adv. Mater.* **2015**, *27*, 41−46.
(15) Chen, J.; Zhou, S.; Jin, S.; Li, H.; Zhai, T. Crystal Organometal Halide Perovskites with Promising Optoelectronic Applications. *J. Mater. Chem. C* **2016**, *4*, 11−27.
(16) Xie, C.; You, P.; Liu, Z.; Li, L.; Yan, F. Ultrasensitive Broadband Phototransistors Based on Perovskite/Organic-Semiconductor Vertical Heterojunctions. *Light: Sci. Appl.* **2017**, *6*, e17023.
(17) Ullah, M.; Tandy, K.; Yambem, S. D.; Muhieddine, K.; Ong, W. J.; Shi, Z.; Burn, P. L.; Meredith, P.; Li, J.; Namdas, E. B. Efficient and Bright Polymer Light Emitting Field Effect Transistors. *Org. Electron.* **2015**, *17*, 371−376.
(18) Cicoira, F.; Santato, C. Organic Light Emitting Field Effect Transistors: Advances and Perspectives. *Adv. Funct. Mater.* **2007**, *17*, 3421−3434.
(19) Santato, C.; Cicoira, F.; Martel, R. Organic Photonics: Spotlight on Organic Transistors. *Nat. Photonics* **2011**, *5*, 392−393.
(20) Zhang, C.; Chen, P.; Hu, W. Organic Light-Emitting Transistors: Materials, Device Configurations, and Operations. *Small* **2016**, *12*, 1252−1294.
(21) Song, L.; Hu, Y.; Zhang, N.; Li, Y.; Lin, J.; Liu, X. Improved Performance of Organic Light-Emitting Field-Effect Transistors by Interfacial Modification of Hole-Transport Layer/Emission Layer: Incorporating Organic Heterojunctions. *ACS Appl. Mater. Interfaces* **2016**, *8*, 14063−14070.
(22) Song, L.; Hu, Y.; Liu, Z.; Lv, Y.; Guo, X.; Liu, X. Harvesting Triplet Excitons with Exciplex Thermally Activated Delayed Fluorescence Emitters toward High Performance Heterostructured Organic Light-Emitting Field Effect Transistors. *ACS Appl. Mater. Interfaces* **2017**, *9*, 2711−2719.
(23) Ullah, M.; Tandy, K.; Li, J.; Shi, Z.; Burn, P. L.; Meredith, P.; Namdas, E. B. High-Mobility, Heterostructure Light-Emitting Transistors and Complementary Inverters. *ACS Photonics* **2014**, *1*, 954−959.
(24) Melucci, M.; Favaretto, L.; Zambianchi, M.; Durso, M.; Gazzano, M.; Zanelli, A.; Monari, M.; Lobello, M. G.; De Angelis, F.; Biondo, V.; et al. Molecular Tailoring of New Thieno(Bis)Imide-Based Semiconductors for Single Layer Ambipolar Light Emitting Transistors. *Chem. Mater.* **2013**, *25*, 668−676.
(25) Capelli, R.; Toffanin, S.; Generali, G.; Usta, H.; Facchetti, A.; Muccini, M. Organic Light-Emitting Transistors with an Efficiency That Outperforms the Equivalent Light-Emitting Diodes. *Nat. Mater.* **2010**, *9*, 496−503.
(26) Schols, S.; Verlaak, S.; Rolin, C.; Cheyns, D.; Genoe, J.; Heremans, P. An Organic Light-Emitting Diode with Field-Effect Electron Transport. *Adv. Funct. Mater.* **2008**, *18*, 136−144.
(27) Dong, H.; Zhu, H.; Meng, Q.; Gong, X.; Hu, W. Organic Photoresponse Materials and Devices. *Chem. Soc. Rev.* **2012**, *41*, 1754−1808.
(28) Namdas, E. B.; Ledochowitsch, P.; Yuen, J. D.; Moses, D.; Heeger, A. J. High Performance Light Emitting Transistors. *Appl. Phys. Lett.* **2008**, *92*, 183304.
(29) Li, D.; Hu, Y.; Zhang, N.; Lv, Y.; Lin, J.; Guo, X.; Fan, Y.; Luo, J.; Liu, X. Near-Infrared to Visible Organic Upconversion Devices Based on Organic Light-Emitting Field Effect Transistors. *ACS Appl. Mater. Interfaces* **2017**, *9*, 36103−36110.
(30) Song, L.; Hu, Y.; Li, D.; Chen, H.; Liu, X. Pixeled Electroluminescence from Multilayer Heterostructure Organic Light-Emitting Transistors. *J. Phys. Chem. C* **2015**, *119*, 20237−20243.
(31) Su, Z. High-Performance Organic Small-Molecule Panchromatic Photodetectors. *ACS Appl. Mater. Interfaces* **2015**, *7*, 2529.
(32) Du, L.; Luo, X.; Zhao, F.; Lv, W.; Zhang, J.; Peng, Y.; Tang, Y.; Wang, Y. Toward Facile Broadband High Photoresponse of Fullerene Based Phototransistor from the Ultraviolet to the near-Infrared Region. *Carbon* **2016**, *96*, 685−694.
(33) Wang, Y.-F.; Qu, F.-D.; Zhou, J.-R.; Guo, W.-B.; Dong, W.; Liu, C.-X.; Ruan, S.-P. High Responsivity Organic Ultraviolet Photodetector Based on Npb Donor and C60 Acceptor. *Chin. Phys. Lett.* **2015**, *32*, 088504.
(34) Zhu, H. L.; Choy, W. C. H.; Sha, W. E. I.; Ren, X. Photovoltaic Mode Ultraviolet Organic Photodetectors with High on/Off Ratio and Fast Response. *Adv. Opt. Mater.* **2014**, *2*, 1082−1089.

DOI: 10.1021/acs.jpcc.8b04320
J. Phys. Chem. C 2018, 122, 15190−15197

(35) Kang, H.-S.; Choi, C.-S.; Choi, W.-Y.; Kim, D.-H.; Seo, K.-S. Characterization of Phototransistor Internal Gain in Metamorphic High-Electron-Mobility Transistors. *Appl. Phys. Lett.* **2004**, *84*, 3780−3782.
(36) Xu, Y.; Berger, P. R.; Wilson, J. N.; Bunz, U. H. F. Photoresponsivity of Polymer Thin-Film Transistors Based on Polyphenyleneethynylene Derivative with Improved Hole Injection. *Appl. Phys. Lett.* **2004**, *85*, 4219−4221.
(37) Jung, J. H.; Yoon, M. J.; Lim, J. W.; Lee, Y. H.; Lee, K. E.; Kim, D. H.; Oh, J. H. High-Performance UV-Vis-NIR Phototransistors Based on Single-Crystalline Organic Semiconductor-Gold Hybrid Nanomaterials. *Adv. Funct. Mater.* **2017**, *27*, 1604528.
(38) Park, J.-E.; Mukherjee, B.; Cho, H.; Kim, S.; Pyo, S. Flexible N-Channel Organic Phototransistor on Polyimide Substrate. *Synth. Met.* **2011**, *161*, 143−147.
(39) Gao, L.; Ge, C.; Li, W.; Jia, C.; Zeng, K.; Pan, W.; Wu, H.; Zhao, Y.; He, Y.; He, J.; et al. Flexible Filter-Free Narrowband Photodetector with High Gain and Customized Responsive Spectrum. *Adv. Funct. Mater.* **2017**, *27*, 1702360.
(40) Noh, Y.-Y.; Kim, D.-Y.; Yoshida, Y.; Yase, K.; Jung, B.-J.; Lim, E.; Shim, H.-K. High-Photosensitivity P-Channel Organic Phototransistors Based on a Biphenyl End-Capped Fused Bithiophene Oligomer. *Appl. Phys. Lett.* **2005**, *86*, 043501.
(41) Xu, H.; Li, J.; Leung, B. H. K.; Poon, C. C. Y.; Ong, B. S.; Zhang, Y.; Zhao, N. A High-Sensitivity Near-Infrared Phototransistor Based on an Organic Bulk Heterojunction. *Nanoscale* **2013**, *5*, 11850−11855.
(42) Tachibana, H.; Aizawa, N.; Hidaka, Y.; Yasuda, T. Tunable Full-Color Electroluminescence from All-Organic Optical Upconversion Devices by Near-Infrared Sensing. *ACS Photonics* **2017**, *4*, 223−227.
(43) Wang, X.; Huang, J.; Li, J.; Yu, J. Effect of Organic Electron Blocking Layers on the Performance of Organic Photodetectors with High Ultraviolet Detectivity. *J. Phys. D: Appl. Phys.* **2016**, *49*, 075102.
(44) Dutta, S.; Narayan, K. S. Nonexponential Relaxation of Photoinduced Conductance in Organic Field Effect Transistors. *Phys. Rev. B: Condens. Matter Mater. Phys.* **2003**, *68*, 125208.
(45) Cho, M. Y.; Kim, S. J.; Han, Y. D.; Park, D. H.; Kim, K. H.; Choi, D. H.; Joo, J. Highly Sensitive, Photocontrolled, Organic Thin-Film Transistors Using Soluble Star-Shaped Conjugated Molecules. *Adv. Funct. Mater.* **2008**, *18*, 2905−2912.

DOI: 10.1021/acs.jpcc.8b04320
J. Phys. Chem. C 2018, 122, 15190−15197